Rare Earth (La, Pr and Sm) Doped Sr1-yCo1-xFexO3 as Cathode in SOFC

Selene Díaz-González , Roberto Campana * , Rocío Andújar , Adrián Pardo , Beatriz Gil-Hernández , Antonio D. Lozano-Gorrín *

Posted Date: 5 December 2023

doi: 10.20944/preprints202312.0280.v1

Keywords: perovskite; solid state; rare earth; Rietveld refinement; SOFC

Article

Rare Earth (La, Pr and Sm) Doped $Sr_{1-y}Co_{1-x}Fe_xO_3$ as Cathode in SOFC

Selene Díaz-González [1], Roberto Campana [2,*], Rocío Andújar [2], Adrián Pardo [2], Beatriz Gil-Hernández [1] and Antonio D. Lozano-Gorrín [1,*]

[1] Departamento de Química, U.D. Química Inorgánica, Universidad de La Laguna, 38200 La Laguna, Tenerife, Spain; adlozano@ull.edu.es

[2] Centro Nacional del Hidrógeno 13500 Puertollano, Spain; roberto.campana@cnh2.es

* Correspondence: roberto.campana@cnh2.es; adlozano@ull.edu.es. Tel.: +34 926 42 06 82

Abstract: This study focuses on the synthesis, characterization and study of a new perovskite-type materials as cathode in SOFC. The synthesized doped perovskites have been successfully synthesized with high purity. The electrochemical performance of these materials was extensively examined through the characterization of I-V-P and EIS curves at the three temperatures: 750, 800 and 850 °C. Where it is revealing a substantial reduction of total resistances by approximately 50% and 70%, accompanied by an impressive increase in power densities by around 200% and 300%, respectively. The cell featuring $Sm_{0.01}Sr_{0.99}Fe_{0.5}Co_{0.5}O_3$ exhibited the most commendable electrochemical properties at each temperature, following closely were $Pr_{0.01}Sr_{0.99}Fe_{0.5}Co_{0.5}O_3$ and $La_{0.01}Sr_{0.99}Fe_{0.5}Co_{0.5}O_3$.

Keywords: perovskite; solid state; rare earth; Rietveld refinement; SOFC

1. Introduction

Within the segment formed by renewable energies, new energy generation systems have become important over recent years, where Solid Oxide Fuel Cells (SOFC) stands out, since they have the advantage of being able to directly convert chemical energy stored in fuels (hydrogen, natural gas or biogas) into electrical energy with high efficiency. Electrode-supported fuel cells have operating temperatures around 600-800 °C, while electrolyte-supported require higher temperatures, usually above 900 °C. Nevertheless, solid oxide systems need to improve their durability, as the high temperatures to which they are subjected induce diffusion processes of species through the component materials, which results in losses in their electrochemical performance and compromises their durability over long periods of operation. For this reason, it is necessary look for new materials for electrodes with high catalytic activity and stability for SOFC [1,2].

Perovskite materials are crystalline compounds with a particular structure that have become very popular in scientific research in recent years due to their amazing electrical and optical properties [3–8]. The structure is characterized by a particular arrangement of the ions within it, which allows a great variety of possible chemical combinations and great potential for its application in electronic and photovoltaic devices. The general formula is ABO_3, where A is a metal ion and B is a nonmetal ion [9].

Regarding the chemical characteristics, perovskites are stable at high temperatures and pressures, and are resistant to corrosion [10–12]. However, some perovskites are sensitive to moisture and light. In terms of structural features, it has a cube-shaped crystal structure, with a large metal ion surrounded by a group of small ions. This structure is responsible for the excellent electronic and mechanical properties of perovskites. In addition, its structure is highly flexible, which allows its properties to be modified through changes in the chemical composition [13,14].

Perovskites have shown to be promising materials due to their unique conductive and semiconducting properties. It has been shown that perovskites can act as active electrodes and catalysts in SOFCs [15–19], allowing for improved cell performance and stability. However, there are still significant challenges to overcome before perovskites can be used in SOFCs in a practical way.

 doi:10.20944/preprints202312.0280.v1

These challenges include the long-term stability of perovskites, the synthesis of high-quality perovskites, and the understanding of charge transport mechanisms in SOFC perovskites.

Starting from the fact that one of the best electrolytes used so far is YSZ due to its magnificent properties, the cathode used must have: a high electronic and ionic conductivity, a high porosity to allow the flow of oxygen and a catalytic activity to be able to to reduce oxygen and generate oxide ions [20–23]. Although one might think that noble metals such as platinum could perform this function, they present a high cost and limitations in the reduction process. It is very common to used samarium doped ceria (SDC) or gadolinium doped ceria (GDC) as protective layer between the electrolyte and the cathode, in order to prevent the formation of poorly conducting secondary phases, which reduced the oxygen electrode performance [24].

The commercialization of SOFC technology depends largely on the improvement of the durability and cost reduction of the cells, where the manufacturing methods have a great relevance. The selection of a suitable fabrication method for each component of planar SOFC usually depends on the cell structure and whether the SOFC are electrolyte-supported or electrode-supported, where fast, economic and environmentally methods are required [25].

To produce anode supported SOFC, one of the most commonly used method is tape casting, due to its low cost and the fact that expensive tools are not needed [26–28]. On the other hand, the deposition of the layers is usually made by different techniques such as chemical vapor deposition, screen printing or dip coating. Wet Powder Spraying (WPS) is considered a promising alternative that allows to control the morphologies and the layer thickness with the advantage of being a low-cost technique [24,29]. In our work three anode-supported cells have been fabricated by a tape casting method. The aim of this research is to study the influence of the use of differente cathodes using self-made powders obtained by freeze-drying. The deposition of the different layers (yttria-stabilized zirconia, YSZ, as electrolyte, gadolinium doped ceria, GDC, as protective layer and $RE_{0.01}Sr_{0.99}Fe_{0.5}Co_{0.5}O_3$ (RE=Pr, La, Sm) as cathode) has been done by WPS, optimizing the deposition procedure. The samples were characterized by X-ray diffraction (XRD) and Scanning Electron Microscopy (SEM). Electrochemical measurements were performed and analyzed.

2. Materials and Methods

2.1. Experimental materials

The reagents were used without further purification: $SrCO_3$ (Aldrich, 99.9%), Fe_2O_3 (Panreac, 96%) and $CoCO_3{\cdot}H_2O$ (Acros Organics, 99%), Pr_6O_{11} (Aldrich, 99.9%), La_2O_3 (Merck, 99.9%), $Sm(NO_3)_3{\cdot}6H_2O$ (Aldrich, 99.9%), YSZ (3%Y, Tosoh), $Gd(NO_3)_3{\cdot}6H_2O$, $Ce(NO_3)_3{\cdot}6H_2O$, NiO (Chemlab, 99%).

2.2. Preparation of material

The method used was freeze-drying where cation solutions must be at basic pH. In addition, and according to what was described by Marrero D. [30], 0.5: 1 ratio of EDTA with respect to metal were added. Once removed from the lyophilizer, the samples were calcined immediately at 850 °C for 4 hours and subsequently heated at 1050 °C for 24 hours.

SOFC´s measurements had been realized in National Hydrogen Center and the procedure was carried out according to Wain-Martin method [16].

For the manufacture of the supports, 3 tapes with a diameter of 24 mm were cut and later they were assembled using a Collin model P200E hot plate press, which is programmable in pressure, temperature and time (20 bar at 115 °C for 60 seconds). Then, the supports were pre-sintered in air before being used for YSZ spraying. In Figure 1 are shown the photographs of the green support (left) and the sintered completed cells (right) with a diameter of 17 mm.

 doi:10.20944/preprints202312.0280.v1

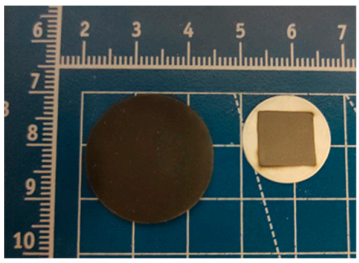

Figure 1. Photograph of the top view of the green tape (left) and top view of the completed cells (right).

The cells have a porous anode made by Ni-YSZ (8% mol Y_2O_3 stabilized ZrO_2), a 10 μm YSZ electrolyte, 2 μm GDC as a protective barrier and a porous cathode made with $RE_{0.01}Sr_{0.99}Fe_{0.5}Co_{0.5}O_3$ (RE=Pr, La, Sm) of 25 μm of thickness. The cathode area was 1 cm2 for performance test. In order to prevent the formation of poorly conducting secondary phases between the electrolyte and cathode layers a protective barrier of GDC has been added.

The deposition of the different layers has been carried out by manual WPS using an Iwata Eclipse HP-BCS airbrush. For the preparation of the inks, the starting powders were ground using a ball mil with a dispersant for 24 hours, adding 2-propanol as solvent.

2.3. Characterization

The diffractograms were performed with an Empyrean PANalytical X-ray diffractometer with Cu Kα1 radiation (α = 1.54056 Å) in a range of 2θ from 10° to 80°. The phase identification was done using the X'Pert HighScore Plus program using the PDF-4 database.

Scanning Electron Microscopy (SEM) studies were carried out at SEGAI (Servicio General de Apoyo a la Investigación) with ZEISS EVO 15 (2nm resolution with 50mm2 Oxford X-MAX Microanalyzer for X-ray Dispersive Energy (EDX)).

In order to perform the electrochemical test, Pt paste was added into the cathode and anode of each sample to improve the contact between the cells and Ni and Au collectors. The cells were mounted on a Open FlangesTM Test Set (Fiaxell) attached by a spring-loaded mechanism. Then, in order to separate the anode and cathode chambers, Mica Phlogopite Paper was used as sealant. Electrochemical measurements were collected using a Potentiostat/Galvanostat VSP (Biologic) coupled to a Booster VMP3 (Biologic), using H2 (3 vol% H2O) as fuel gas on the anodic side and air on the cathodic one at temperatures of 750, 800 and 850 °C. The flow rates were set at 2 L/h for H_2 and 6 L/h for air and the polarization applied to the impedance test was 50 mA.

3. Results and discussions

3.1. X-Ray Powder Patterns

The XRD patterns are shown in Figure 2. This data presented are consistent with cubic phase, and space group $Pm\bar{3}m$ with hkl positions illustrated in Table 1. As can be seen, when the proportions of the atoms are changed, the peaks shift slightly to larger angles. This phenomenon is due to the difference in ionic radio of the atoms in the structure and how they are introduced into it due to the atomic dispersion factor.

Preprints (www.preprints.org) | NOT PEER-REVIEWED | Posted: 5 December 2023 doi:10.20944/preprints202312.0280.v1

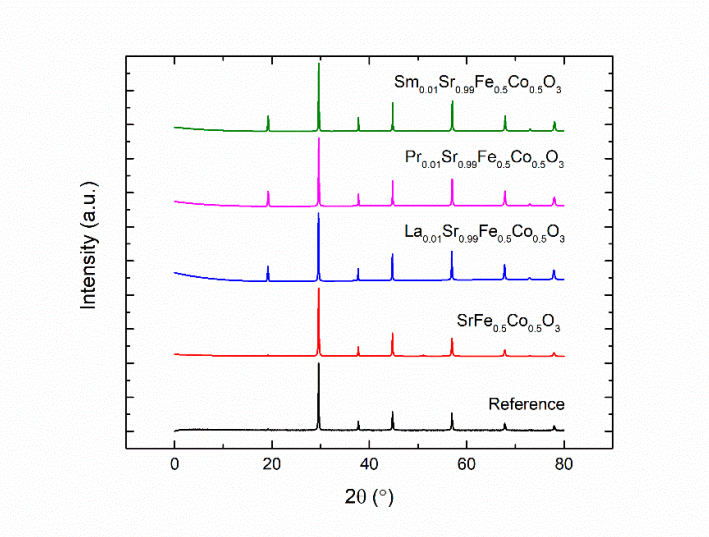

Figure 2. X-ray difraction patterns of samples (in colours) and their comparative with database (in black).

Table 1. hkl positions.

Hkl positions										
h	1	1	1	2	2	2	2	3	2	2
k	0	1	1	0	1	1	2	0	2	1
l	0	0	1	0	0	1	0	0	1	0
2θ	22.9	32.7	40.3	46.9	52.8	58.3	68.5	73.3	73.3	78.0

The cell parameters and reliability factors obtained from Rietveld refinements are shown in Table 2. The differences in cell volume are explained by the fact that iron atoms have a larger radius in the case of the first three samples; while in the doped samples, the difference is due to the atoms that share a hole with strontium. The factors obtained from the Rietveld refinement are comparable to the bibliography consulted for this type of phase, so it is considered an optimal refinement for all samples.

Table 2. Cell parameters and reliability factors.

Sample	**a (Å)**	**V(Å³)**	**R_{Bragg}**	**R_p**	**R_{wp}**	**R_{exp}**	**X^2**
$SrFe_{0.5}Co_{0.5}O_3$	3.862	57.635	2.27	33.1	20.8	7.30	8.12
$Sr_{0.99}La_{0.01}Fe_{0.5}Co_{0.5}O_3$	3.870	57.979	1.85	82.8	39.4	27.08	2.12
$Sr_{0.99}Pr_{0.01}Fe_{0.5}Co_{0.5}O_3$	3.868	57.915	0.036	37.6	25.7	7.50	11.7
$Sr_{0.99}Sm_{0.01}Fe_{0.5}Co_{0.5}O_3$	3.865	57.765	0.0141	60.3	37.1	11.07	11.2

3.2. Morphological analysis

The morphology of the prepared materials was characterized by SEM. To see it in a better way, each atom has been colored with a different color (Figure 3). A homogeneous surface is observed in all samples and Table 3 shows the EDX analyzes in which the proportions of the atoms are confirmed.

Preprints (www.preprints.org) | NOT PEER-REVIEWED | Posted: 5 December 2023 doi:10.20944/preprints202312.0280.v1

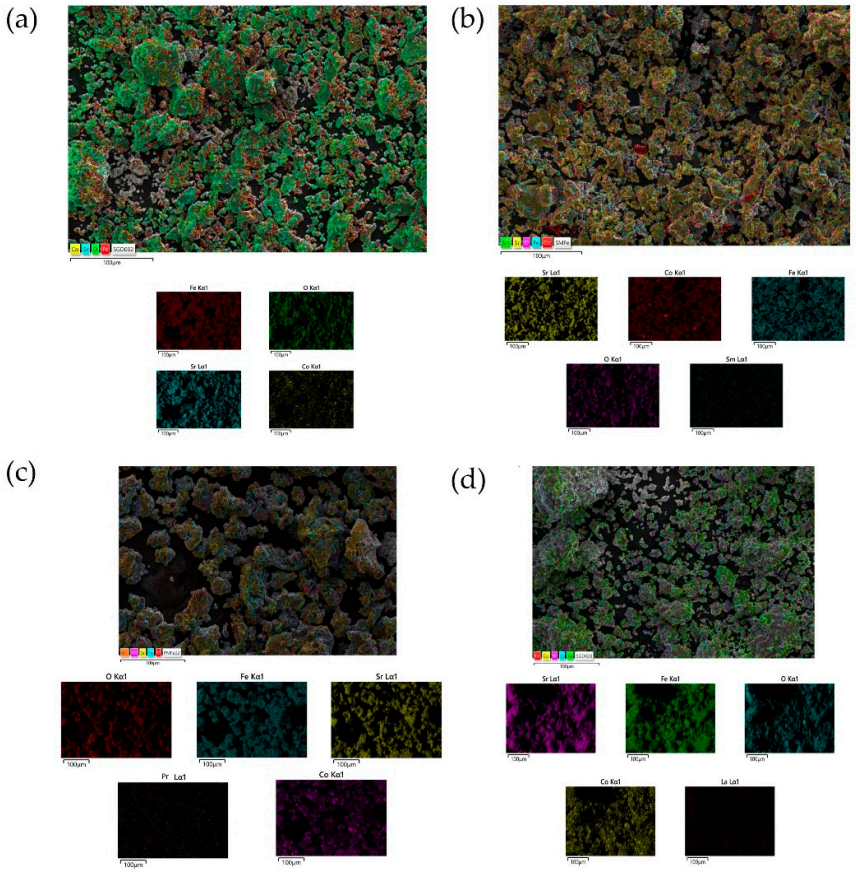

Figure 3. SEM images of: **(a)** $SrFe_{0.5}Co_{0.5}O_3$; **(b)** $Sr_{0.99}Sm_{0.01}Fe_{0.5}Co_{0.5}O_3$; **(c)** $Sr_{0.99}Pr_{0.01}Fe_{0.5}Co_{0.5}O_3$; **(d)** $Sr_{0.99}La_{0.01}Fe_{0.5}Co_{0.5}O_3$.

Table 3. EDX analysis.

Sample	%Sr	%Fe	%Co	%O	% other
$SrFe_{0.5}Co_{0.5}O_3$	35.43	30.93	9.63	24.01	-
$Sr_{0.99}La_{0.01}Fe_{0.5}Co_{0.5}O_3$	31.59	27.71	16.97	16.97	1.07
$Sr_{0.99}Pr_{0.01}Fe_{0.5}Co_{0.5}O_3$	35.63	27.35	13.57	22.48	0.97
$Sr_{0.99}Sm_{0.01}Fe_{0.5}Co_{0.5}O_3$	21.11	17.02	38.01	22.20	1.06

Finally, SEM images of the built piles have been obtained, in which all the layers can be perfectly observed (Figure 4). It should be noted that these images were after the measurements, so one can ensure that they have not undergone degradation.

Preprints (www.preprints.org) | NOT PEER-REVIEWED | Posted: 5 December 2023 doi:10.20944/preprints202312.0280.v1

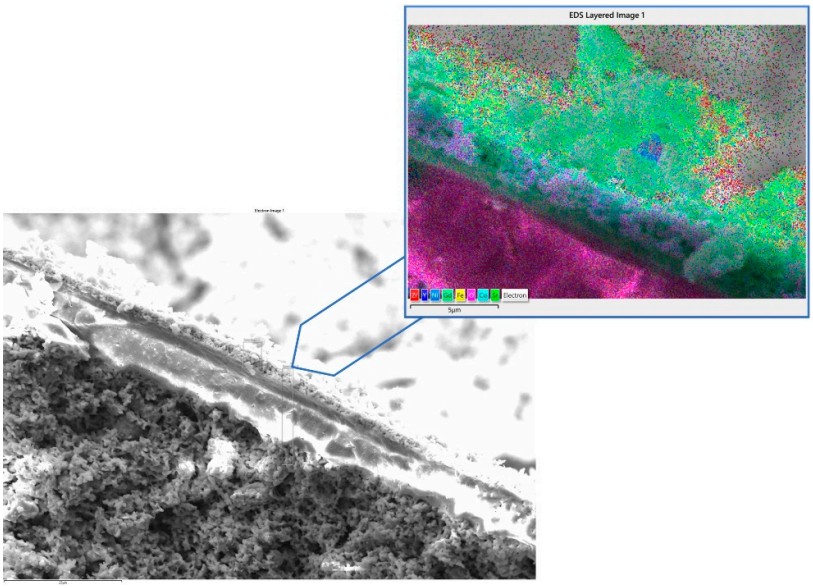

Figure 4. SEM image of one of the samples where it observed four layers. Each layer is Ni-YSZ, YSZ, GDC and perovskite.

3.3. Cell electrochemical characterization

Polarization curves were performed at maximum current densities of 52 mA·cm^{-2} at each of the samples for temperatures of 750, 800 and 850 °C. Ideal working way would have been to reach current densities to obtain a potential of 0.6 V, as this fact had not possible, extrapolation of the data is performed assuming that the slope of the obtained curves remains constant. In this way, the polarization curves obtained are shown by attaching the obtained values after extrapolation. The impedance measurements were performed at 50 mA with deacreasing frequency from 100 kHz to 1 Hz, with an amplitude of 10 mA.

The cells described have been characterized as a function of temperature: 750, 800 and 850 °C. The current-voltage and current-power characteristics of the cells at these temperatures are given in Figure 5. The obtained open circuit voltage (OCV) is the predicted by the Nernst Equation (1.10 V at 750 °C), except in sample with $La_{0.01}Sr_{0.99}Fe_{0.5}Co_{0.5}O_3$ as cathode. It is observed that a change in working temperature significantly affects electrochemical properties. The increase of the working temperature favors a decrease in the resistance, and as a consequence, an increase in the working power density.

Figure 5a shows polarization curves of $La_{0.01}Sr_{0.99}Fe_{0.5}Co_{0.5}O_3$ as cathode, it can be seen that obtained resistances and maximum power densities are 10.58, 5.38 and 3.24 Ω·cm^2, and 21.90, 38.23 and 59.84 mW·cm^{-2} to 750, 800 and 850 °C, respectively. It is also observed that the OCV of 0.93 V is lower than the 1.10 V expected by the Nernst equation, it is probably due to small leakages in the mica sheet used as sealant. This fact affects the measured potencial and, as a consequence, the maximum power density that the cell is able to generate.

Preprints (www.preprints.org) | NOT PEER-REVIEWED | Posted: 5 December 2023 doi:10.20944/preprints202312.0280.v1

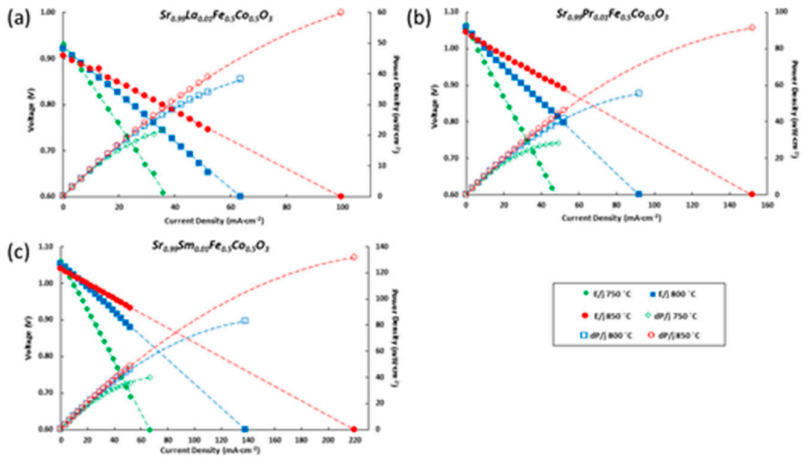

Figure 5. (I-V-P) curves of the cells at 750, 800 and 850 °C using: **(a)** $Sr_{0.99}La_{0.01}Fe_{0.5}Co_{0.5}O_3$; **(b)** $Sr_{0.99}Pr_{0.01}Fe_{0.5}Co_{0.5}O_3$; **(c)** $Sr_{0.99}Sm_{0.01}Fe_{0.5}Co_{0.5}O_3$ as cathode.

In Figure 5b, polarization curves of $Sr_{0.99}Pr_{0.01}Fe_{0.5}Co_{0.5}O_3$ cathode, own resistances and maximum power densities are 9.55, 4.68 and 2.81 Ω·cm², and 28.30, 55.25 and 91.24 mW·cm-2 to 750, 800 and 850 °C, respectively. His OCV is 1.07 V, newly a similar value to expect by the Nernst equation.

Lastly, Figure 5c that´s for $Sr_{0.99}Sm_{0.01}Fe_{0.5}Co_{0.5}O_3$ as cathode, had resistances 7.14, 3.37 and 2.04 Ω·cm² and maximum power densities 39.92, 82.82 and 131.82 mW·cm^{-2} to 750, 800 and 850 °C, respectively. As in the previous case, OCV is 1.06 V, which brings back, a result similar to Nernst equation.

Figure 6 shows, for each material, its EIS diagram as a function of temperatures. In all cases a trend is observed: when the temperature increses, the values of real Z axis decrease. This means that the ohmic drop, the activation of the electrodes as well as the difussion processes, are thermally activated. From the EIS spectra is possible to obtain the ohmic resistance using the intersection values with the Z real axis at high frequencies, as expected the ohmic resistance, mainly associated with the YSZ electrolyte, remained almost constant for the three cells. In the case of the total resistance, value that include ohmic and polarisation resistances, can be obtained from the intersection of the diagram with the Z real axis in the low frecuencies zone. Polarization resistances, generally associated with gas phase diffusion processes, decrease when the temperature decrese.

From the EIS spectra is possible to obtain the ohmic resistance using the intersection values with the Z real axis at high frequencies. We are able to compare them with similar cells already studied, which are collected in Table 4.

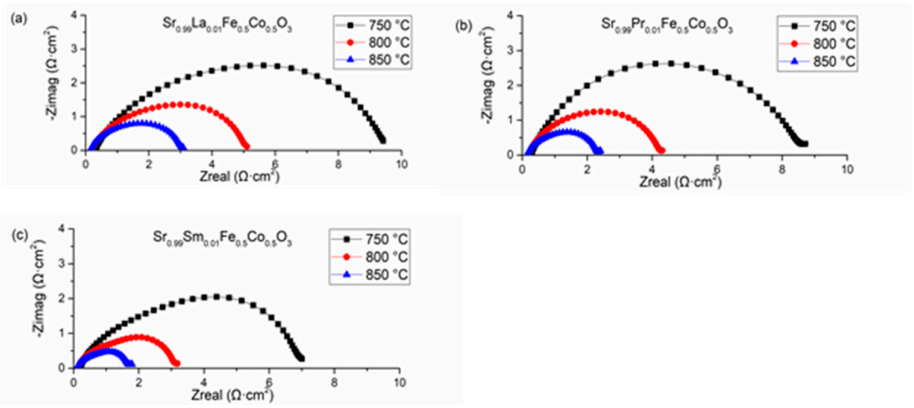

Figure 6. Nyquist diagrams at 750, 800 and 850 °C using: **(a)** $Sr_{0.99}La_{0.01}Fe_{0.5}Co_{0.5}O_3$; **(b)** $Sr_{0.99}Pr_{0.01}Fe_{0.5}Co_{0.5}O_3$; **(c)** $Sr_{0.99}Sm_{0.01}Fe_{0.5}Co_{0.5}O_3$ as cathode.

Preprints (www.preprints.org) | NOT PEER-REVIEWED | Posted: 5 December 2023 doi:10.20944/preprints202312.0280.v1

Table 4. Ohmic and polarization resistances obtained from the EIS of the cells at 750, 800 and 850 °C.

Temperature		$Sr_{0.99}La_{0.01}Fe_{0.5}Co_{0.5}O_3$	$Sr_{0.99}Pr_{0.01}Fe_{0.5}Co_{0.5}O_3$	$Sr_{0.99}Sm_{0.01}Fe_{0.5}Co_{0.5}O_3$
750 °C	R_{ohm} (Ω·cm²)	0.33	0.28	0.20
	R_{pol} (Ω·cm²)	9.09	8.43	6.86
	R_{total} (Ω·cm²)	9.42	8.71	7.07
800 °C	R_{ohm} (Ω·cm²)	0.21	0.20	0.13
	R_{pol} (Ω·cm²)	4.89	4.10	3.04
	R_{total} (Ω·cm²)	5.10	4.30	3.18
850 °C	R_{ohm} (Ω·cm²)	0.15	0.14	0.09
	R_{pol} (Ω·cm²)	2.93	2.25	1.69
	R_{total} (Ω·cm²)	3.09	2.40	1.79

According to the data obtained, the resistance to polarization of our materials improves as we increase the temperature and, furthermore, it is better for the compound doped with samarium than with praseodymium and lanthanum. Although it is true that analogous systems doped with lanthanum are among the most studied, it is observed that samarium, under the same conditions, represents an improvement. Obtained polarization results of studied cells at 800 °C show values of 5.10, 4.30 and 3.18 for $Sr_{0.99}La_{0.01}Fe_{0.5}Co_{0.5}O_3$, $Sr_{0.99}Pr_{0.01}Fe_{0.5}Co_{0.5}O_3$ and $Sr_{0.99}Sm_{0.01}Fe_{0.5}Co_{0.5}O_3$, respectively. Compared to other bibliographic studies such $Ba_{0.09}Co_{0.7}Fe_{0.2}Nb_{0.1}O_3$ system [31], $Sr_{0.4}La_{0.6}Fe_{0.8}Cu_{0.2}O_3$ system [32], and others similar works as $Sr_{0.4}La_{0.4}Ni_{0.2}Fe_{0.8}O_3$ compound [33] and $Sr_{0.5}Ba_{0.5}Zn_{0.2}Fe_{0.8}O_3$ sample [34], Our results show slightly lower electrochemical performances, however, we can assure that our material is promising but still needs microstructural optimization to increase the response of the fabricated electrodes.

4. Conclusions

The synthesized doped perovskites have been successfully synthesized with high purity. In addition, the results of I-V-P and EIS curves characterization verified very good electrochemical performance of these materials at the three temperatures studied. It has been demonstrated that in all cases when temperature was increased from 750 to 800 and 850 °C we obtained those total resistances were reduced approximately by 50 and 70%, and power densities were incremented approximately by 200% and 300%, respectively. As expected, these cells work better when temperature is increased. Cell with $Sr_{0.99}Sm_{0.01}Fe_{0.5}Co_{0.5}O_3$ as cathode shows the best electrochemical properties at each temperature, followed by $Sr_{0.99}Pr_{0.01}Fe_{0.5}Co_{0.5}O_3$ and $Sr_{0.99}La_{0.01}Fe_{0.5}Co_{0.5}O_3$. The results obtained for cell with $Sr_{0.99}Sm_{0.01}Fe0.5Co_{0.5}O_3$ (ohmic polarization of 0.09 Ω·cm², OCV of 1.06 V, total resistances of 1.79 Ω·cm² and maximum power densities of 131.82 mA·cm^{-2} at 850 °C) have demonstrated optimal electrochemical parameters to use these types of material as cathode of SOFCs. It is believed necessary to continue the study of cells with $Sr_{0.99}La_{0.01}Fe_{0.5}Co_{0.5}O_3$ as cathode to confirm if low OCV values are taken as valid or if they are due to small leakages in the mica sheet used as sealant.

Author Contributions: Conceptualization, R.C.,S.D.,A.D.,B.G.; methodology, S.D.,R.C., R.A, A.P.; software, S.D., R.A, A.P.; validation, S.D.,A.D.; formal analysis, S.D., A.D.; investigations, R.C., R.A, A.P.; resources, R.C..; data curation, R.C., R.A, A.P.; writing—original draft preparation, S.D.,R.C., R.A.; writing—review and editing, R.C., S.D.,A.D,B.G,R.A..; visualization, R.C., R.A, A.P.; supervision, R.C.A.D.,B.G.; project administration, A.D., R.C.; funding acquisition, R.C. All authors have read and agreed to the published version of the manuscript.

Funding: This research was funded by Complementary Renewable Energy and Hydrogen Plan of the Recovery, Transformation and Resilience Plan funded by the European Union - Next Generation-EU, grant number C17.I01.P01.

Data Availability Statement: Data presented in this study are available on request from the corresponding author.

Conflicts of Interest: The authors declare no conflict of interest.

References

1. Choudhury, A. Application of solid oxide fuel cell technology for power generation. *Renew. Sust. Energ. Rev.,* **2013**, *20*, 430-442. https://doi.org/10.1016/j.rser.2012.11.031.
2. Esposito, V.; Garbayo, I; Linderoth, S.; Pryds, N. Epitaxial Growth of Complex Metal Oxides. *Solid-oxide fuel cells,* **2015**, 443-478. https://doi.org/10.1016/B978-1-78242-245-7.00015-4.
3. Chen, D.; Chen, X. Luminiscent perovskite quantum dots: synthesis, microstructures, optical properties and application. *J. Mater. Chem. C.,* **2019**, *7*, 1413-1446. https://doi.org/10.1039/C8TC05545A.
4. Shamsi, J.; Urban, A.S.; Imran, M.; De Trizio, L.; Manna, L. Metal Halide Perovskite Nanocrystals: Synthesis, Post-Synthesis Modifications, and Their Optical Properties. *Chem. Rev.,* **2019**, *119*, 3296-3348. https://doi.org/10.1021/acs.chemrev.8b00644
5. Bera, S.; Pradhan, N. Perovskite Nanocrystal Heterostructures: Synthesis, Optical Properties, and Applications. *ACS Energy Lett.,* **2020**, *5*, 2858-2872. https://doi.org/10.1021/acsenergylett.0c01449.
6. Rodríguez-Romero, J.; Clasen Hames, B.; Galar, P.; Fakharuddin, A.; Suarez, I.; Schmidt-Mende, L.; Martínez-Pastor, J. P.; Douhal, A.; Mora-Seró, I.; Barea, E. M. Tuning optical/electrical properties of 2D/3D perovskite by the inclusion of aromatic cation. *Phys. Chem. Chem. Phys.,* **2018**, *20*, 30189-30199. https://doi.org/10.1039/c8cp06418k.
7. Yang, F.; Li, M.; Li, L.; Wu, P.; Pradal-Velázquez, E.; Sinclair, D. C. Defect chemistry and electrical properties of sodium bismuth titanate perovskite. *J. Mater. Chem. A,* **2018**, *6*, 5243-5254. https://doi.org/10.1039/c7ta09245h.
8. Schade, L.; Wright, A. D.; Johnson, R. D.; Dollmann, M.; Wenger, B.; Nayak, P. K.; Prabhakaran, D.; Herz, L. M.; Nicholas, R.; Snaith, H. J.; Radaelli, P. G. Structural and Optical Properties of Cs2AgBiBr6 Double Perovskite. *ACS Energy Lett.,* **2019**, *4*, 299-305. https://doi.org/10.1021/acsenergylett.8b02090.
9. Smith, A. J.; Welch, A. J. E. , Some Mixed Metal Oxides of Perovskite Structure. *Acta Cryst.,* **1960**, *13*, 653. https://doi.org/10.1107/S0365110X60001540.
10. Luo, P.; Liu, Z.; Xia, W.; Yuan, C.; Cheng, J.; Lu, Y. Uniform, Stable and Efficient Planar-Hterojunction Perovskite Solar Cells by Facile Low-Pressure Chemical Vapor Deposition under Fully Open-Air conditions. ACS Appl. Mater. *Interfaces,* **2015**, *7*, 2708-2714. https://doi.org/10.1021/am5077588.
11. Sunarso, J.; Hashim, S. S.; Zhu, N.; Zhou, W. Perovskite oxides applications in high temperature oxygen separation, solid oxide fuel cell and membrane reactor: A review. *Prog. Energy Combust. Sci.,* **2017**, *61*, 57-77. https://doi.org/10.1016/j.pecs.2017.03.003.
12. Kaus, I.; Wiik, K.; Krogh, B.; Dahle, M.; Hofstad, K. H.; Aasland, S. Stability of SrFeO3-Based Materials in H20/CO2-Containing Atmospheres at High Temperatures and Pressures. *J. Am. Ceram. Soc.,* **2007**, *90*, 2226-2230. https://doi.org/10.1111/j.1551-2916.2007.01727.x.
13. Klug, M. T.; Osherov, A.; Haghighirad, A. A.; Stranks, S. D.; Brown, P. R.; Bai, S.; Wang, J. T. W.; Dang, X.; Bulović, V.; Snaith, H. J.; Belcher, A. M. Tailoring metal halide perovskites through metal substitution: influence on photovoltaic and material properties. *Energy Environ. Sci.,* **2017**, *10*, 236-246. https://doi.org/10.1039/c6ee03201j.
14. Giorgi, G.; Fujisawa, J. I.; Segawa, H.; Yamashita, K. Cation Role in Structural and Electronic Properties of 3D Organic-Inorganic Halide Perovskites: A DFT Analysis. *J. Phys. Chem. C.,* **2014**, *118*, 12176-12183. https://doi.org/10.1021/jp504479c.
15. Troncoso, L.; Gardey, M. C.; Fernández-Díaz, M. T.; Alonso, J. A. New Rhenium-Doped SrCo1-xRexO3-δ Perovskites Performing as Cathode In Solid Oxide Fuel Cells. *Materials,* **2016**, *9*, 1-14. https://doi.org/10.3390/ma9090717.
16. Wain-Martin, A.; Campana, R.; Morán-Ruiz, A.; Larrañaga, A.; Arriortua, M. I. Synthesis and processing of SOFC components for the fabrication and characterization of anode supported cells. *Bol. Soc. Esp. Ceram. V.,* **2022**, *61*, 264-274. https://doi.org/10.1016/j.bsecv.2020.11.008.
17. Marcucci, A.; Zurlo, F.; Sora, I. N.; Placidi, E.; Casciardi, S.; Licoccia, S.; Di Bartolomeo, E. A redox stable Pd-doped perovskite for SOFC applications. *J. Mater. Chem. A.,* **2019**, *7*, 5344-5352. https://doi.org/10.1039/c8ta10645b.
18. Grunbaum, N.; Mogni, L.; Prado, F.; Caneiro, A. Phase equilibrium and electrical conductivity of SrCo0.8Fe0.2O3-δ. *J. Solid State Chem.,* **2004**, *177*, 2350-2357. https://doi.org/10.1016/j.jssc.2004.03.026.
19. Wang, Z.; Zhao, H.; Xu, N.; Shen, Y.; Ding, W.; Lu, X.; Li, F. Electrical conductivity and structural stability of SrCo1-xFexO3-δ. *J. Phys. Chem. Solids,* **2011**, *72*, 50-55. https://doi.org/10.1016/j.jpcs.2010.10.084.
20. Mogensen, M.; Skaarup, S. Kinetic and geometric aspects of solid oxide fuel cell electrodes. *Solid State Ion.,* **1996**, *86-88*, 1151-1160. https://doi.org/10.1016/0167-2738(96)00280-9
21. Simner, S. P.; Anderson, M. D.; Pederson, L. R.; Stevenson, J.W. Performance variability of La(Sr)FeO3 SOFC Cathode with Pt, Ag, and Au Current Collectors. *J. Electrochem. Soc.,* **2005**, *152*, A1851. https://doi.org/10.1149/1.1995687.
22. Mogensen, M.; Jensen, K. V.; Jørgensen, M.J.; Primdahl, S. Progress in understanding SOFC electrodes. *Solid State Ion.,* **2002**, *150*, 123-129. https://doi.org/10.1016/S0167-2738(02)00269-2.

23. Nielsen, J.; Hjelm, J. Impedance of SOFC electrodes: A review and a comprehensive case study on the impedance of LSM: YSZ cathodes. *Electrochim. Acta,* **2014**, *115*, 31-45. https://doi.org/10.1016/j.electacta.2013.10.053.
24. Z. Pan, Q. Li, M. Ni, R. Lyu, P. Li, S.H. Chan. Activation and failure mechanism of La0.6Sr0.4Co0.2Fe0.8O3-δ air electrode in solid oxide electrolyzer cells under high-current electrolysis. *Int. J. Hydrogen Energ.*, **2018**, *43*, 5437-5450. https://doi.org/10.1016/j.ijhydene.2018.01.181.
25. Wain-Martin, A.; Morán-Ruiz, A.; Laguna-Bercero, M.A.; Campana, R.; Larrañaga, A.; Raimond Slater, P.; Arriortua, M.I. SOFC cathodic layers using wet powder spraying technique with self synthesized nanopowders. *Int. J. Hydrog. Energy*, **2019**, *44*, 7555-7563. https://doi.org/10.1016/j.ijhydene.2019.01.220.
26. Jabbari, M.; Bulatova, R.; Tok, A.I.; Bahl, C.R.H.; Mitsoulis, E.; Hattel, J.H. Ceramic tape casting: A review of current methods and trends with emphasis on rheological behaviour and flow analysis. *Mat. Sci. Eng. B*, **2016**, *212*, 39-61. https://doi.org/10.1016/j.mseb.2016.07.011.
27. Wang, Z.; Qian, J.; Cao, J.; Wang, S.; Wen, T. A study of multilayer tape casting method for anode-supported planar type solid oxide fuel cells (SOFCs). *J. Alloys Compd.,* **2007**, *437*, 264-268. https://doi.org/10.1016/j.jallcom.2006.07.110.
28. Song, J.H.; Park, S.I.; Lee, J.H.; Kim, H.S. Fabrication characteristics of an anode-supported thin-film electrolyte fabricated by the tape casting method for IT-SOFC. *J. Mater. Process. Technol.*, **2008**, *198*, 414-418. https://doi.org/10.1016/j.jmatprotec.2007.07.030
29. Carpanese, M.P.; Barbucci, A.; Canu, G.; Viviani, M. BaCe0.85Y0.15O0.295 dense layer by wet powder spraying as electrolyte for SOFC/SOEC applications. *Solid State Ion.,* **2015**, *269*, 80-85. https://doi.org/10.1016/j.ssi.2014.11.014
30. Marrero López, D., Síntesis y caracterización de nuevos conductores iónicos basados en La2Mo2O9, Tesis Doctoral. Universidad de La Laguna, España, 2006.
31. Yang, Z.; Yang, C.; Jin, C.; Han, M.; Chen, F. Ba0.9Co0.7Fe0.2Nb0.1O3-δ as cathode material for intermediate temperature solid oxide fuel cells. *Electrochem Commun*, **2011**, *13*, 882-885. https://doi.org/10.1016/J.ELECOM.2011.05.029.
32. Zhou, Q.; Xu, L.; Guo, Y.; Jia, D.; Li, Y.; Wei, W.C.J. La0.6Sr0.4Fe0.8Cu0.2O3-δ perovskite oxide as cathode for IT-SOFC. *Int. J. Hydrogen Energy*, **2012**, *37*, 119363-11968. https://doi.org/10.1016/J.IJHYDENE.2012.05.114.
33. Zhu, G.; Fang, X.; Liu, X. Preparation and electrical properties of La0.4Sr0.6Ni0.2Fe0.8O3 using a glycine nitrate process. *Ceram. Int.,* **2005**, *31*, 115-119. https://doi.org/10.1016/J.CERAMINT.2004.03.042.
34. Qiu, P.; Jia, L.; Chi, B.; Pu, J.; Li, J.; Chen, F. LaCoO3-δ coated Ba0.5Sr0.5Co0.8Fe0.2O3-δ cathode for intermediate temperature solid oxide fuel cells. *Electrochim. Acta,* **2019**, *319*, 981-989. https://doi.org/10.1016/J.ELECTACTA.2019.07.054.